JACS
JOURNAL OF THE AMERICAN CHEMICAL SOCIETY

Communication

pubs.acs.org/JACS

Quantitative Chemical Imaging with Multiplex Stimulated Raman Scattering Microscopy

Dan Fu,[†] Fa-Ke Lu,[†] Xu Zhang,[‡] Christian Freudiger,[†] Douglas R. Pernik,[§] Gary Holtom,[†] and Xiaoliang Sunney Xie*,[†]

[†]Department of Chemistry and Chemical Biology, Harvard University, Cambridge, Massachusetts 02138, United States

[‡]School of Engineering and Applied Sciences, Harvard University, Cambridge, Massachusetts 02138, United States

[§]Department of Chemical and Biomolecular Engineering, University of Notre Dame, Notre Dame, Indiana 46556, United States

Supporting Information

ABSTRACT: Stimulated Raman scattering (SRS) microscopy is a newly developed label-free chemical imaging technique that overcomes the speed limitation of confocal Raman microscopy while avoiding the nonresonant background problem of coherent anti-Stokes Raman scattering (CARS) microscopy. Previous demonstrations have been limited to single Raman band measurements. We present a novel modulation multiplexing approach that allows real-time detection of multiple species using the fast Fourier transform. We demonstrate the quantitative determination of chemical concentrations in a ternary mixture. Furthermore, two imaging applications are pursued: (1) quantitative determination of oil content as well as pigment and protein concentration in microalgae cultures; and (2) 3D high-resolution imaging of blood, lipids, and protein distribution in ex vivo mouse skin tissue. We believe that quantitative multiplex SRS uniquely combines the advantage of fast label-free imaging with the fingerprinting capability of Raman spectroscopy and enables numerous applications in lipid biology as well as biomedical imaging.

Raman spectroscopy is a powerful technique for noninvasive characterization of both biological and nonbiological samples. To obtain spatially resolved chemical information, the confocal Raman technique can be employed. However, spontaneous Raman scattering is intrinsically weak and is unsuitable for high-speed imaging. Coherent anti-Stokes Raman scattering (CARS) offers orders-of-magnitude higher sensitivity, and video-rate imaging has been achieved.[1] However, it has a nonresonant background problem that originates from a four-wave mixing process.[2] New developments in CARS microscopy have removed the nonresonant background problem by using complicated experimental procedures or postimage data processing.[3] Most recently, stimulated Raman scattering (SRS) microscopy has emerged as an alternative to CARS microscopy.[4−8] Unlike CARS, SRS microscopy has straightforward image interpretation and quantification without the complications arising from nonresonant background and phase-matching conditions. Consequently, not only is the signal-to-noise ratio (SNR) improved, but the Raman spectral fidelity is also preserved. Because SRS has a linear concentration dependence, it has the potential to become a powerful method for label-free quantitative determination of chemical concentrations of individual species in a multicomponent system.

A major limitation of the current implementation of SRS microscopy is that only a single Raman band can be probed at a time. To measure quantitatively multiple components with overlapping Raman bands, at least the same number of bands must be measured. However, as high-sensitivity SRS imaging uses a high-frequency lock-in detection scheme, the same spectrally resolved detection approach that is commonly employed in fluorescence and multiplex CARS detection is currently impractical to implement because of the difficulty of building a multichannel lock-in amplifier that works in the megahertz frequency range.[9−11] Spectrally tailored excitation is an excellent way of circumventing this problem that can distinguish as many chemical components as the number of spectral elements.[12] However, this technique is restricted to detection of a single species per imaging session and requires all species to be externally calibrated before imaging.

Here we present a novel modulation multiplexing approach that allows multiple Raman bands to be measured simultaneously (Figure 1). Through either in situ calibration or external calibration, multispecies chemical mapping can be implemented at subcellular resolution with speeds at least 3 orders of magnitude faster than for confocal Raman imaging. To detect multiple Raman bands simultaneously, a broadband Ti:sapphire femtosecond laser is used in place of the picosecond laser as the pump. The femtosecond laser is divided into a number of wavelength bands, with each band corresponding to one Raman shift that is modulated at its own RF frequency. This is achieved with an acousto-optical tunable filter device (AOTF, Crystal Technology). The filtered pump beam is then combined with an electrically synchronized picosecond laser at 1064 nm and sent to a laser scanning microscope (Olympus Fluoview 300). The exact Raman shift is determined by the energy difference between the filtered pump beam and the Stokes beam, which is encoded in the modulation frequency. By means of a Fourier transform approach, individual Raman bands are extracted by demodulation at different frequencies and therefore can be measured simulta-

Received: October 26, 2011
Published: February 8, 2012

   dx.doi.org/10.1021/ja210081h | J. Am. Chem. Soc. 2012, 134, 3623−3626

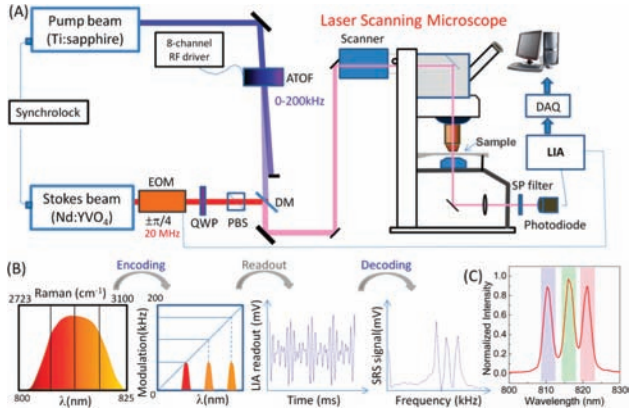

Figure 1. (A) Schematic diagram of the multiplex SRS setup. QWP, quarter-wave plate; EOM, electro-optical modulator; PBS, polarizing beamsplitter; DM, dichroic mirror; PMT, photomultiplier tube; LIA, lock-in amplifier; DAQ, data acquisition card. (B) Workflow of the multiplex Raman encoding and decoding process. (C) Example AOTF-filtered spectrum using three-channel modulation. Each shaded region corresponds to one channel modulated at a particular frequency.

neously. The spectral resolution of each band is limited by the AOTF to 33 cm^{-1}.

We first demonstrated the quantitative determination of chemical concentrations of a ternary solution system. Mixtures of three chemicals with significant Raman band overlap in the CH stretching region (oleic acid, cholesterol, and cyclohexane) were dissolved in deuterated chloroform. A total of nine binary and three ternary mixtures were prepared. We chose three Raman peaks to probe (2850, 2900, and 2960 cm^{-1}) on the basis of their spontaneous Raman spectra (shown in Figure 2A). The power in each channel was 16 mW, and the Stokes power was 76 mW at the objective focus. A standard linear algebra operation was used to calculate the binary and ternary mixture concentrations on the basis of measurements on single species. A ternary plot of the calculated concentrations is shown in Figure 2B. We can see that the concentrations of most of the solutions were correctly inferred. The residual errors we see in the ternary plot are largely caused by femtosecond laser spectral drift during the measurement, synchronization timing jitter, and the inaccuracy of the matrix calibration due to cross-talk of the three channels caused by AOTF diffraction sidelobes. The measurement accuracy would be significantly improved if the timing jitter and cross-talk were eliminated with better modulation technology.

We note that the multiplex data acquisition can be carried out at a rate of >5 kHz, which is at least 2 orders of magnitude higher than the rate of either conventional Raman imaging or multiplex CARS imaging. Moreover, for spatially segregated samples, calibration can be obtained in situ using the three-channel images. To demonstrate this capability, we imaged mixtures of three different polymer beads embedded in agarose gel: 2 μm polystyrene (PS), 1−10 μm poly(methyl methacrylate) (PMMA), and 2 μm melamine. Three images (512 × 512 pixels with 200 μs pixel dwell time) were generated simultaneously. Figure 2D shows the composite image of the three channels at 2950, 3000, and 3050 cm^{-1}, represented in red, blue, and green, respectively. The red and blue channels exhibit small differences due to the similar Raman spectra of melamine and PMMA. To distinguish them clearly, we first constructed the calibration matrix using in situ imaging data

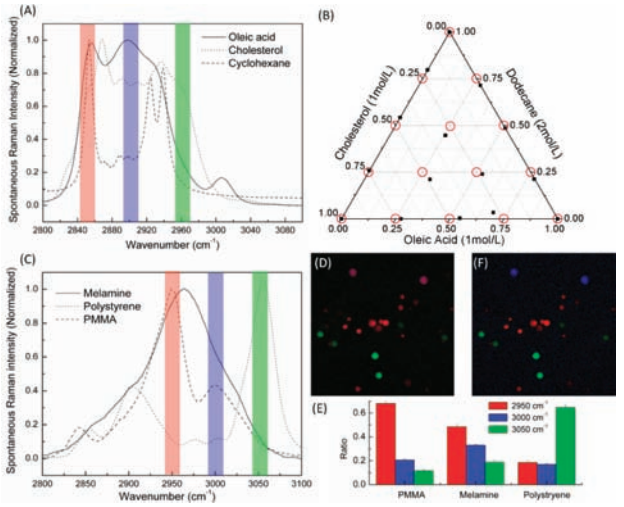

Figure 2. (A) Spontaneous Raman spectra of oleic acid, cholesterol, and cyclohexane. The red, blue, and green lines indicate the locations of the three Raman bands used for multiplex SRS imaging. (B) Ternary plot of the calculated concentrations of the three-component mixture based on the multiplex SRS measurement. (C). Spontaneous Raman spectra of melamine, PMMA, and polystyrene beads. (D) Raw composite SRS image; red, blue, and green represent the images at 2950, 3000, 3050 cm^{-1}, respectively. (E) Calibration bar graph showing the normalized Raman intensities of each kind of bead at the three designated Raman bands. (F) Reconstructed Raman image (red, PMMA; blue, melamine; green, polystyrene).

from three different kinds of beads and then applied the inverse matrix to the three-channel image. Figure 2E shows the normalized matrix values for the three different kinds of beads in a bar graph. It agrees very well with that of spontaneous Raman spectra of the three species shown in Figure 2C. The calculated concentration images were recompiled into an RGB composite image with each color showing one species (Figure 2 F). The different beads can now be readily distinguished.

In the first application, we demonstrated the use of multiplex SRS to study microalgae biochemical composition, especially lipid content. The need for renewable energy sources has sparked growing interest in green algae oil production.[13,14] The lipids (mainly triglycerides) stored in the microalgae could be converted into biodiesel efficiently. Various methods have been employed to evaluate the genetic and environmental factors that affect the oil-producing capability of microalgae, but all have significant drawbacks. Fluorescent probes face problems such as nonspecific labeling, inaccuracy in quantification, photobleaching, and phototoxicity.[15] Traditional biochemical methods such as chromatography and mass spectrometry cannot analyze single cells and do not allow continuous in situ monitoring of oil accumulation. Most recently, Raman microspectroscopy has been used to study algal lipid composition but with very low throughput.[16] CARS and SRS are excellent label-free alternatives for investigating lipid content because lipids are usually concentrated in droplets and have very strong Raman signals,[17,18] whereas chlorophyll and carotenoids (both called "pigment" from here on), which are abundant in green algae, have strong two-color two-photon absorption (TPA) that interferes with Raman imaging. In addition, it is important to separate the protein from the lipids quantitatively, which is not possible with single Raman band imaging. TPA is a related nonlinear optical process that generates a modulation signal in this pump−probe-type

dx.doi.org/10.1021/ja210081h | J. Am. Chem. Soc. 2012, 134, 3623−3626

imaging experiment, but it has a much broader spectral response than Raman scattering.[19] With our new multiplex SRS approach, three channels can be used to separate pigment TPA, lipid SRS, and protein SRS.

Microalgae cultures were imaged using three different bands: 2780, 2850, and 2940 cm^{-1}. TPA contributes to all three channels because of its broad spectral response. At 2780 cm^{-1}, the protein and lipid signals are almost negligible. At 2850 cm^{-1}, the lipids have a large Raman signal, and at 2940 cm^{-1}, both the lipids and the protein have strong Raman signals. We calibrated the signal distribution in the three channels from the protein and the lipids using two prepared samples, 30% bovine serum albumin solution and liquid oleic acid (Sigma). For pigment calibration, we used the obtained experimental images, similar to the calibration process used in the bead imaging. Cell cultures of *Botryococcus Braunii* microalgae were grown in modified bold 3N medium (both from UTEX). We compared two different lighting conditions: continuous illumination versus a 12 h:12 h light:dark cycle. The optical power was lowered to 22 mW for the pump beam (all three channels) and 40 mW for the Stokes beam to minimize photodamage due to TPA. Figure 3A shows an example raw composite image of the

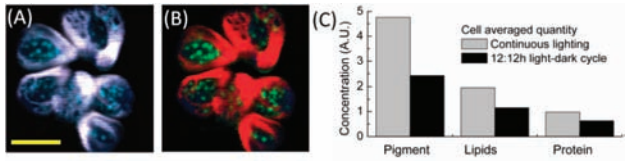

Figure 3. Multiplex SRS imaging of microalgal cells under different illumination conditions. (A) Raw composite images of microalgal cells using three bands: 2780 cm^{-1} (red), 2850 cm^{-1} (green), and 2940 cm^{-1} (blue). (B) Corresponding unmixed images: chlorophyll and carotenoids (red), lipids (green), and protein (blue). (C) Bar graph of cell-averaged concentrations of pigment, lipids, and protein for the two different samples. Scale bar: 10 μm.

SRS + TPA signal of microalgae. We can see that the pigment signal dominates all three channels but is mostly located at the periphery of the cell in a clamshell shape, whereas lipid droplets are concentrated in the center of the cell. After unmixing of the spectra, the image clearly distinguishes the three major components (Figure 3B). We took a total of 15 frames for each sample (see the Supporting Information). With thresholding methods, the sizes of the cells were calculated. The average cell size for the continuous-illumination sample was much larger than that for 12 h:12 h light:dark cycle sample lighting (data not shown). It is known that algal cells under intense illumination can attain higher biomass than cells adapted to low-level irradiance.[20] To be more quantitative, we compared the cell-averaged biomasses for the two different types. Figure 3C shows a bar graph of the results. There was an increase in cellular concentration for all three components when the microalgae were grown under continuous illumination. In particular, pigment increased by 95%, lipids by 68%, and protein by 56%. The oil content can be gauged by the fraction of lipid mass in the total cell mass. We used the ratio of lipids to protein as a semiquantitative measure of the oil content. Clearly, under continuous lighting, the lipid/protein ratio in the cell increased. This result was corroborated by other studies.[21,22] Interestingly, the pigment content increased the most. This is probably due to the adaptation of algal cells to light to increase their photosynthetic activities.

In the second application, we showed that multiplex SRS could be used to study complicated biological samples for which calibration of individual components is not easily available. In those cases, it is useful to use the spatial features of a sample to create pseudobasis sets (assuming selected spatial locations have only one of the three major components) and use the images themselves to construct the calibration matrix. Consequently, the calculated images may not reflect the absolute concentrations of each individual chemical component but should still reflect the contributions of the major components. To demonstrate this, we imaged the 3D structure of mouse skin tissue. Skin has a very complicated structure and composition, providing both barrier and transport functions. These functions are intimately associated with vasculature and lipids. As discussed previously, the 2850 cm^{-1} channel mainly has contributions from lipids, while the 2940 cm^{-1} channel has contributions from both lipids and proteins.[8] The 2780 cm^{-1} channel is off Raman resonance and provides contrast for two-color TPA of hemoglobin, a key species that allows visualization of blood vessels.[19,23] By using an independent channel to characterize the contribution from blood, together with lipids and protein SRS signals, we were able to disentangle the major biochemical compositions at different skin layers. The calibration matrix was obtained by picking specific regions with features corresponding to protein layers, blood vessels, and subcutaneous fat layers based on raw composite images at different imaging depths. After reconstruction, Figure 4 shows

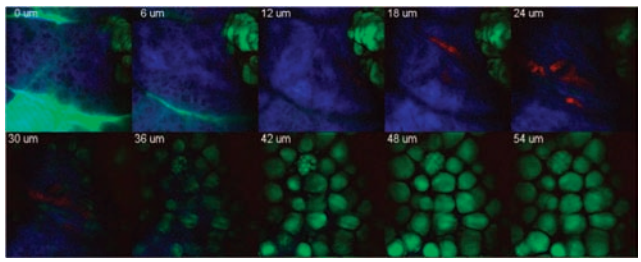

Figure 4. Multiplex SRS *z*-stack images of freshly excised mouse ear skin tissue: red, blood contrast; green, lipid contrast; blue, protein contrast. Each image is 512 × 512 pixels.

spectrally separated blood (red), lipid (green), and protein (blue) images at increasing imaging depths with a 6 μm depth increment. Qualitatively, we can observe spatially distinctive features for blood vessels at a depth of 15−30 μm. The lipid layer on the surface and the fat layer in the hypodermis can be clearly identified. We can also see that in the epidermis, there are many large cell nuclei (with characteristic low lipid concentrations), and some have visible nucleoli, as marked by higher protein content. Within the fat cell layer, some fat cells are surrounded by large numbers of much smaller lipid droplets. Those exquisite features are indications of the high sensitivity and spatial resolution of our multiplex SRS method. This capability offers the potential for label-free real-time digital pathology.

In conclusion, we have presented multiplex SRS imaging using a novel modulation multiplex approach. Double modulation and double demodulation are employed to achieve high speed and high sensitivity. Combining the advantages of high-speed label-free imaging and the chemical fingerprinting power of Raman spectroscopy, multiplex SRS is a powerful and quantitative method for fast label-free chemical composition analysis in biological systems. In comparison with sequential

dx.doi.org/10.1021/ja210081h | *J. Am. Chem. Soc.* 2012, 134, 3623−3626

wavelength tuning-based SRS, multiplex SRS is faster and more reliable. In addition, any sample movement on the subsecond scale creates difficulties in image registration and renders quantitative analysis invalid for sequential imaging but only distorts images in multiplex SRS. The speed of multiplex SRS is currently limited by the modulation speed of the AOTF, but it could be further improved by 2 orders of magnitude (up to 500 kHz) with other technologies, such as a multichannel acousto-optical modulator. With such a modulator, the sensitivity and measurement accuracy could also be significantly improved as a result of better resolution (possibly <15 cm^{-1}) and a larger number of channels (up to eight or 16, depending on the model). The number of components that can be analyzed increases linearly with the number of spectral channels.

Our demonstrated applications focused on the C−H stretching region because C−H stretching offers a strong SRS signal and it is critical to have multiplex SRS for discriminating different species in this strongly congested vibrational region. Eight- or 16-channel SRS could enable quantification of different lipid species such as triglycerides and cholesterol esters. Extending multiplex modulation to the fingerprint region would be straightforward by tuning the Ti: sapphire laser to >900 nm. The SNR of multiplex SRS is only slightly degraded in comparison to narrowband SRS as a result of cross-talk. Therefore, all previous coherent Raman applications demonstrated in the fingerprint region can be better implemented by multiplex SRS with better chemical specificity and quantitative multicomponent analysis. It is worth mentioning that there is a delicate balance between laser bandwidth, number of spectral channels, and spectral information. Ideally, the larger the spectral bandwidth and the number of channels, the better is the selectivity can be achieved. However, the laser power at each individual band is limited, resulting in a corresponding degradation of the SNR. We believe that with proper design, multiplex SRS has enormous potential for use as a label-free chemical imaging approach for studying complex systems. It will find important applications in lipid biology and biomedical imaging.

■ ASSOCIATED CONTENT

Ⓢ Supporting Information

Detailed descriptions of the experimental setup, data analysis, and high-resolution imaging results. This material is available free of charge via the Internet at http://pubs.acs.org.

■ AUTHOR INFORMATION

Corresponding Author

xie@chemistry.harvard.edu

■ ACKNOWLEDGMENTS

We thank Dr. Xiaohui Ni for providing the mouse skin sample. This work was supported by the NIH T-R01 (1R01EB010244-01) Award to X.S.X.

■ REFERENCES

(1) Evans, C. L.; Xie, X. S. *Annu. Rev. Anal. Chem.* **2008**, *1*, 883.
(2) Cheng, J. X.; Xie, X. S. *J. Phys. Chem. B* **2004**, *108*, 827.
(3) Day, J. P. R.; Domke, K. F.; Rago, G.; Kano, H.; Hamaguchi, H.-o; Vartiainen, E. M.; Bonn, M. *J. Phys. Chem. B* **2011**, *115*, 7713.
(4) Ploetz, E.; Laimgruber, S.; Berner, S.; Zinth, W.; Gilch, P. *Appl. Phys. B: Lasers Opt.* **2007**, *87*, 389.
(5) Freudiger, C. W.; Min, W.; Saar, B. G.; Lu, S.; Holtom, G. R.; He, C.; Tsai, J. C.; Kang, J. X.; Xie, X. S. *Science* **2008**, *322*, 1857.
(6) Ozeki, Y.; Kitagawa, Y.; Sumimura, K.; Nishizawa, N.; Umemura, W.; Kajiyama, S. i.; Fukui, K.; Itoh, K. *Opt. Express* **2010**, *18*, 13708.
(7) Nandakumar, P.; Kovalev, A.; Volkmer, A. *New J. Phys.* **2009**, *11*, No. 033026.
(8) Saar, B. G.; Freudiger, C. W.; Reichman, J.; Stanley, C. M.; Holtom, G. R.; Xie, X. S. *Science* **2010**, *330*, 1368.
(9) Muller, M.; Schins, J. M. *J. Phys. Chem. B* **2002**, *106*, 3715.
(10) Cheng, J.-x.; Volkmer, A.; Book, L. D.; Xie, X. S. *J. Phys. Chem. B* **2002**, *106*, 8493.
(11) Kano, H.; Hamaguchi, H.-o *Appl. Phys. Lett.* **2005**, *86*, No. 121113.
(12) Freudiger, C. W.; Min, W.; Holtom, G. R.; Xu, B.; Dantus, M.; Xie, X. S. *Nat. Photonics* **2011**, *5*, 103.
(13) Li, Y.; Horsman, M.; Wu, N.; Lan, C. Q.; Dubois-Calero, N. *Biotechnol. Prog.* **2008**, *24*, 815.
(14) Mata, T. M.; Martins, A. A.; Caetano, N. S. *Renewable Sustainable Energy Rev.* **2010**, *14*, 217.
(15) Elle, I. C.; Olsen, L. C. B.; Pultz, D.; Rodkar, S. V.; Fargeman, N. J. *FEBS Lett.* **2010**, *584*, 2183.
(16) Wu, H.; Volponi, J. V.; Oliver, A. E.; Parikh, A. N.; Simmons, B. A.; Singh, S. *Proc. Natl. Acad. Sci. U.S.A.* **2011**, *108*, 3809.
(17) Nan, X.; Potma, E. O.; Xie, X. S. *Biophys. J.* **2006**, *91*, 728.
(18) Wang, M. C.; Min, W.; Freudiger, C. W.; Ruvkun, G.; Xie, X. S. *Nat. Methods* **2011**, *8*, 135.
(19) Fu, D.; Ye, T.; Matthews, T. E.; Chen, B. J.; Yurtserver, G.; Warren, W. S. *Opt. Lett.* **2007**, *32*, 2641.
(20) Banerjee, A.; Sharma, R.; Chisti, Y.; Banerjee, U. C. *Crit. Rev. Biotechnol.* **2002**, *22*, 245.
(21) Darzins, A.; Hu, Q.; Sommerfeld, M.; Jarvis, E.; Ghirardi, M.; Posewitz, M.; Seibert, M. *Plant J.* **2008**, *54*, 621.
(22) Fabregas, J.; Maseda, A.; Dominguez, A.; Ferreira, M.; Otero, A. *Biotechnol. Lett.* **2002**, *24*, 1699.
(23) Fu, D.; Matthews, T. E.; Ye, T.; Piletic, I. R.; Warren, W. S. *J. Biomed. Opt.* **2008**, *13*, No. 040503.